Response to Reviewer 1

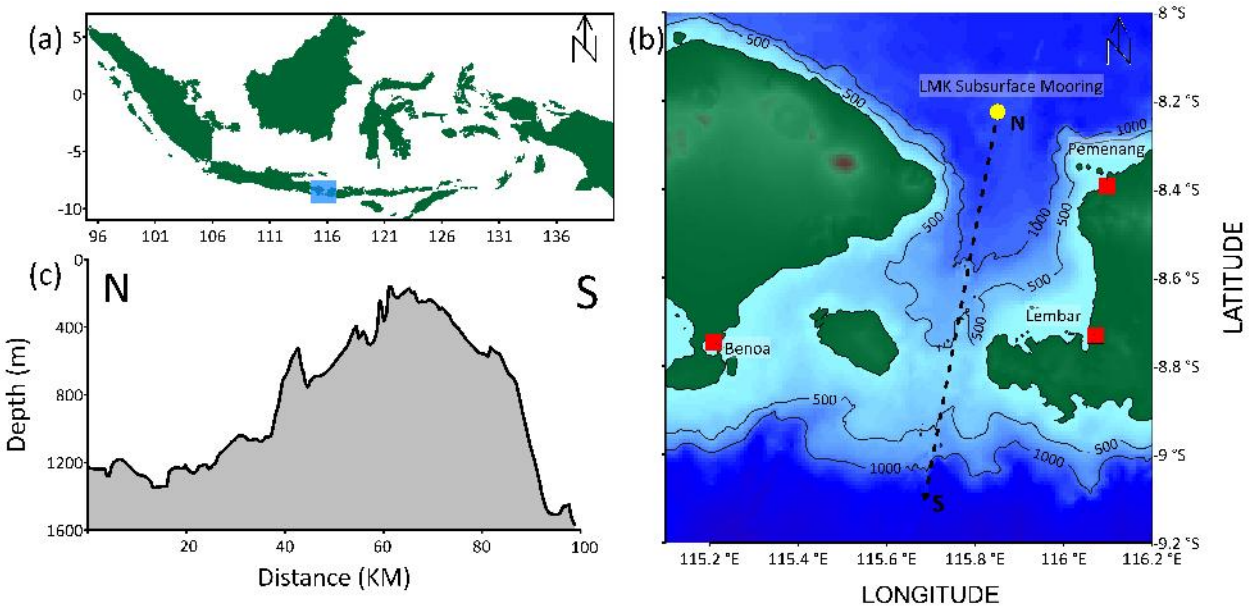
We thank the reviewer for the constructive assessment. Each point is addressed below.

Catalogue revision. While addressing the comments we re-examined the event catalogue and found that it included elevation-type (upward) isotherm displacements in addition to depression-type solitons, although the manuscript stated that only depression-type events were retained. These signals (176 of 617 detected solitons, 78 of them in August–September 2024) had no clear velocity signature in the ADCP record and were concentrated in months when the 18°C isotherm was near the top of the sampled depth range. We removed them. The catalogue now contains 258 packets and 441 solitons, and all statistics and figures were recomputed. The conclusions are unchanged; the main differences are that the secondary August maximum in packet counts disappears and that the event-scale correlations of amplitude with ITF velocity and effective phase speed are slightly stronger (r = +0.27 and +0.29, previously +0.21 and +0.20).

Major Comment 1: Geographic and mooring location context

The manuscript lacks a geographic focus figure showing the mooring location, bathymetry of the Lombok Strait, the sill region, and the surrounding Indonesian archipelago.

Response. We agree. A new Figure 1 has been added. (a) Regional overview of the Indonesian Archipelago; the blue rectangle marks the Lombok Strait region shown in panel (b). (b) Bathymetric map of the Lombok Strait and surrounding seas. The yellow circle marks the LMK subsurface mooring site (8°13′S, 115°51′E), which is also the northern end of the N–S section. Red squares indicate the tide gauge stations at Pemenang, Lembar and Benoa. The dashed line (N–S) shows the bathymetric transect plotted in panel (c). (c) Along-strait bathymetric profile along the N–S transect, extending ~100 km from the Bali Sea (N) to the Indian Ocean (S) and showing the sill complex, the primary ISW generation site. Bathymetry is from the GEBCO 2025 Grid (GEBCO Compilation Group, 2025, doi:10.5285/37c52e96-24ea-67ce-e063-7086abc05f29).



Major Comment 2: What is genuinely new beyond satellite observations?

The authors need to more forcefully articulate and demonstrate what the mooring data reveal that satellite data cannot (propagation direction; mode-2 or higher-mode waves; periodicity tied to the tidal cycle).

Response. We thank the reviewer for these three specific suggestions. We carried out each analysis with the mooring data, and we revised the Introduction to state what the mooring adds.

(a) Propagation direction. We determined the direction of each packet from the wave-induced velocity measured by the ADCP (2-minute sampling). For depression-type packets with a clear velocity signal, 90% propagated northward with a mean bearing of 17°, and all 17 extreme packets with ADCP data propagated northward. The remaining 10% (18 packets) showed a weak southward velocity signature. All were small (25–33 m), their wave-induced velocities were close to the noise level, and only 56% showed the upper/lower-layer velocity reversal expected for a mode-1 wave, compared with 87% of the northward packets. Their direction is therefore uncertain. If some are southward-propagating waves, a single mooring cannot identify their source; this is stated in Sect. 4.4. We therefore cannot yet answer whether the two populations respond differently to the ITF: the southward group is too small and too weak for a separate analysis.

(b) Higher modes. The thermistor chain spans only 120 m, which is too short to test for mode-2 waves from temperature. The ADCP covers 60–450 m, and in 84% of the packets the 300–450 m velocity opposed the upper-layer velocity, which is the mode-1 structure. We did not find evidence for mode-2 waves, but we do not claim that they are absent.

(c) Tidal periodicity. Packet occurrence is strongly modulated by the spring–neap cycle (packet rate 5.4 times higher in the spring third of days than in the neap third from the ADCP current, with a similar contrast at the Benoa tide gauge), peak amplitude increases with tidal range ($r = +0.33$), and arrivals of the larger packets are phase-locked to the M2 tide. Monthly M2 amplitude, in contrast, varies little and does not explain the seasonal cycle. Generation is therefore controlled by the tide rather than stochastic, and the background flow modulates which tidal cycles produce extreme waves (see also Comment 4).

Revised text in Sect. 1:

"Satellite imagery records the surface expression of ISWs and therefore integrates over all amplitude classes; it cannot show whether large- and small-amplitude waves respond differently to the background state. Large-amplitude ISWs depart from the weakly nonlinear (Korteweg–de Vries) regime, and their evolution depends on amplitude as well as on the background stratification and shear (Helfrich and Melville, 2006; Lamb, 2014), so such a difference is plausible but has not been tested with in situ data. Beyond subsurface amplitude, a mooring provides three quantities that satellite images do not: the propagation direction and vertical structure of each packet from the wave-induced velocity, the timing of every packet relative to the tide, and the concurrent background velocity profile."

New paragraph in Sect. 3.1:

"Propagation direction and vertical structure were examined for the 217 packets with concurrent ADCP data. The wave-induced velocity was obtained by removing a ±45 min running median from the 80–120 m layer-mean velocity, and its direction at the time of maximum speed within ±10 min of the isotherm peak was taken as the propagation direction, because the upper-layer velocity of a mode-1 depression wave is aligned with its propagation. Of the 179 packets with a signal-to-noise ratio of at least 2, 161 (90%) propagated northward with a mean bearing of 17° (10th–90th percentiles 0°–35°), as expected for waves generated at the sill south of the mooring. All 17 extreme packets with ADCP data propagated northward, with upper-layer wave-induced speeds of 0.6–1.5 m s^{-1}. The remaining 18 packets (10%) had a weak southward signature. All were small (25–33 m), and their wave-induced upper-layer velocities (0.12–0.31 m s^{-1}) were close to the noise level (median signal-to-noise ratio 3.0, against 5.1 for the northward packets). Only 56% of them showed the opposing deep-layer velocity expected for a mode-1 wave, against 87% of the northward packets. Their propagation direction is therefore uncertain; if some of them propagate southward, their source cannot be identified from a single mooring (Sect. 4.4). In 84% of the 179 packets the 300–450 m velocity opposed the upper-layer velocity (lower row of Fig. 3), consistent with a mode-1 structure; the thermistor chain spans only 120 m and cannot be used to test for mode-2 waves."

Revised paragraph at the end of Sect. 3.2:

"Tidal forcing was examined with the ADCP record and coastal tide gauges. The principal axis of the tidal (30-h high-pass) depth-mean (80–450 m) current at the mooring is oriented along 8°, close to north–south. A harmonic fit to its meridional component over the full record gives amplitudes of 0.094 m s^{-1} for M2, 0.042 m s^{-1} for S2, 0.015 m s^{-1} for K1 and 0.013 m s^{-1} for O1. Monthly M2 amplitudes vary only between 0.07 and 0.11 m s^{-1} and are lowest in the months with the most packets ($r = -0.84$, $n = 11$ months), so the seasonal cycle of ISW occurrence is not explained by a seasonal increase in tidal amplitude. The spring–neap cycle, in contrast, has a strong effect. When days are ranked by the standard deviation of the high-passed depth-mean meridional current, the packet rate is 1.02 per day in the upper third (spring tides) and 0.19 per day in the lower third (neap tides), a ratio of 5.4; the Benoa tide gauge gives a similar contrast (1.41 and 0.19 packets per day for the upper and lower thirds of daily tidal range). At the Lembar and Pemenang gauges the contrast in total packet rate is weaker (ratios of 1.7 and 1.4), but at all three gauges at least 80% of the extreme packets fall in the upper third of daily tidal range. None of the 17 extreme packets with ADCP data occurred in the neap third, and 10 occurred in the spring third. Peak amplitude also increases with tidal range ($r = +0.33$, $p < 0.001$, $n = 242$, for the ±12 h tidal range at Pemenang; mean range of 167 cm for extreme and 132 cm for normal packets). Packet arrivals are phase-locked to the semidiurnal tide: packets of 45 m or more arrive on average 145° of M2 phase after maximum northward depth-mean flow at the mooring (mean resultant length 0.76, $n = 52$, Rayleigh test $p < 0.001$). No extreme packet occurred on neap-tide days, whereas the seasonal modulation is not explained by tidal amplitude."

Major Comment 3: Effective phase speed calculation

Why is the two-layer approximation used rather than a continuously stratified formulation? The authors should either justify the two-layer simplification with a sensitivity analysis comparing against continuously stratified solutions, or adopt a more sophisticated method (Taylor–Goldstein equation).

Response. We performed the requested sensitivity analysis. The mooring temperature sensors sampled only about 85–260 m (pressure-corrected depths), so the mooring alone does not give a full-depth density profile. We therefore used a shipboard CTD cast taken at the mooring site (27 November 2025, 7–490 m) together with ADCP mean velocity profiles, and solved the long-wave Taylor–Goldstein equation for mode 1.

The two-layer formula differs from the continuously stratified mode-1 speed by about 3% for this cast. More importantly for our argument, the change in northward mode-1 speed between the record-mean velocity profile and the mean profile around extreme packets is +0.17 m s^{-1} when the vertical shear is included, the same as the +0.17 m s^{-1} obtained from the simple layer-mean (50–200 m) Doppler estimate. Including the shear therefore does not change the size of the effect.

We state the limits of this test in the manuscript: it uses one cast taken a year after the mooring record, the stratification below 490 m is extrapolated, and it is a linear long-wave calculation. We retain the two-layer estimate for the monthly and event-scale statistics because it can be evaluated throughout the record.

> **Revised text in Sect. 4.4:**
>
> "To assess this simplification, we solved the long-wave Taylor–Goldstein equation for the first vertical mode, using the density profile from a shipboard CTD cast at the mooring site (27 November 2025, 7–490 m; stratification below 490 m extrapolated with e-folding scales from 200 m to infinity) and ADCP mean meridional velocity profiles (60–460 m). Without background flow the mode-1 speed is 2.56–2.59 m s^{-1}, compared with 2.50 m s^{-1} from the two-layer formula applied to the same cast (layer densities averaged above and below the 18°C isotherm), a difference of about 3%. With the record-mean velocity profile the northward mode-1 speed is 2.41–2.44 m s^{-1}, and with the mean profile for the ±36 h around extreme packets it is 2.58–2.61 m s^{-1}. This difference of +0.17 m s^{-1} equals the Doppler estimate from the 50–200 m layer-mean velocity (+0.17 m s^{-1}), so including the vertical shear does not change the size of the effect. The test relies on a single cast taken a year after the mooring record, when the 18°C isotherm was at 215 m, and it does not address fully nonlinear effects."

Major Comment 4: Event-scale correlation analysis (Figure 4)

> *The correlation coefficients explain only ~4–5% of the variance, and there is no physical reason to expect a linear relationship. The threshold behaviour is better represented as a conditional probability or threshold analysis.*

Response. We agree, and we added a conditional probability analysis to Sect. 3.4. The text now states that the linear correlations explain only about 8% of the variance. No extreme packet occurred when the thermocline-layer velocity was more southward than −0.13 m s^{-1}, and the fraction of extreme packets rises from 0% to 15% across the three velocity classes.

Following the tidal analysis requested in Comment 2, we also combined the velocity condition with tidal strength. Using the same spring-tide definition as for the packet rates, extreme packets were about four times more frequent when spring tides coincided with a weak or reversed ITF (18% of packets under these conditions against 4.8% otherwise; Fisher exact test $p = 0.004$). The pattern is unchanged when August–September 2024, the months with the poorest isotherm coverage, are excluded.

The scatter plots and linear fits (now Fig. 6) are retained for illustration only.

Revised text in Sect. 3.4:

"A conditional probability analysis quantifies the threshold behaviour. Among the 217 packets with concurrent ADCP records, the fraction that were extreme was 0 of 32 (0%) for V100–250 < −0.15 m s^{-1}, 8 of 127 (6.3%) for −0.15 ≤ V100–250 < 0 m s^{-1}, and 9 of 58 (15.5%) for V100–250 ≥ 0 m s^{-1} (Fisher exact test between the first and third classes, p = 0.02). Combining this with tidal strength, using the same spring-tide definition as in Sect. 3.2 (the upper third of days ranked by tidal-current strength), 9 of the 49 packets (18%) that occurred on spring-tide days with V100–250 ≥ −0.05 m s^{-1} were extreme, compared with 8 of 168 (4.8%) under all other conditions (Fisher exact test, p = 0.004). Extreme packets were therefore about four times more frequent when strong tidal forcing coincided with a weak or reversed ITF, although this combination accounts for only 9 of the 17 extreme packets. Figure 3a, b and d illustrates the contrast for individual packets: under similar weak ITF, a spring-tide day produced an 83 m packet and a neap-tide day a 42 m packet, whereas a spring-tide day with strong southward ITF produced only a 25 m soliton. Excluding August–September 2024, when isotherm coverage was poorest, removes only packets from the two southward-flow classes and leaves the pattern unchanged (0 of 27, 8 of 109 and 9 of 58)."

Major Comment 5: Separation of generation vs. propagation effects

With a single mooring this is admittedly difficult, but the authors should at least acknowledge this limitation explicitly and discuss what additional observations would be needed.

Response. We agree and now state this limitation explicitly in Sect. 4.4. The direction analysis (Comment 2a) shows that the extreme packets arrive from the sill to the south, but it does not tell us whether the background flow acts at generation or during propagation.

Text in Sect. 4.4:

"Second, with a single mooring we cannot observe ISW generation at the sill or track individual packets from the sill to the mooring. Nor can we separate the contributions of (a) ITF-induced modification of tidal energy conversion at the main sill (hydraulic control); (b) enhanced nonlinear steepening during northward propagation when Doppler retardation is reduced; and (c) amplitude-selective dissipation between the sill and the mooring. The inferred hydraulic-control mechanism is consistent with the velocity composites but has not been verified directly. A mooring array with instruments near the sill and at the present site would be required to partition these effects and to observe southward-propagating waves from the northern sill."

Major Comment 6: Amplitude classification thresholds

The basis for the 25 m lower bound is not explained. The 65 m "natural break" should be shown or described more clearly in the main text.

Response. Lower bound. The 25 m threshold is a detection limit. The thermistor spacing is 20 m, and the measured high-frequency variability of the detection isotherm outside wave packets has a standard deviation of 4.5 m, so 25 m exceeds five standard deviations. Events below 25 m were not catalogued, so

we could not test a lower threshold; instead we show that raising the threshold to 30 m or 35 m does not change the results. We acknowledge that smaller ISWs exist and are not counted.

Upper threshold. On re-examining the amplitude distribution we found that it decays approximately exponentially and has no sharp break at 65 m. We have removed the term "natural break". The 65 m threshold is now described as a definition of the high-amplitude tail (about the 90th percentile; 27 of 258 packets), and we report the sensitivity of the results to thresholds between 60 and 70 m. The distribution and the threshold sensitivity are now shown in Appendix A (Fig. A1), which is part of the manuscript rather than the Supplement, so the basis of the threshold is visible in the main article.

The class counts in Sect. 3.1 changed with the catalogue revision described at the top of this letter: small 189 packets (73.3%), moderate 42 (16.3%), extreme 27 (10.5%).

> **Revised text in Sect. 2.2:**
>
> "A lower amplitude threshold of 25 m was applied for two reasons: (1) detection sensitivity—the thermistor spacing is 20 m, and the high-frequency (<1 h) variability of the detection isotherm outside wave packets has a standard deviation of 4.5 m (2.7–7.5 m by month), so a 25 m threshold exceeds five standard deviations of the background variability; and (2) raising the threshold to 30 m or 35 m (175 and 116 packets) leaves the seasonal pattern unchanged and the event-scale ITF–amplitude correlation significant ($r = +0.33$ and $+0.29$, both $p < 0.01$). Events smaller than 25 m were not catalogued, so sensitivity to a lower threshold could not be tested. Extreme ISWs are defined as packets with a peak amplitude above 65 m (27 packets, 10.5%; about the 90th percentile of the packet amplitude distribution). The amplitude distribution decays approximately exponentially without a sharp break (Fig. A1), so the 65 m threshold is a definition of the high-amplitude tail. Varying it between 60 and 70 m changes the number of extreme packets from 34 to 21 (13.2–8.1%), but in every case no extreme packet occurred for $V_{100–250} < -0.15$ m s^{-1} and the Mann–Whitney difference in $V_{100–250}$ between extreme and normal packets remains significant ($p < 0.01$)."

Major Comment 7: Figure quality and readability

All figures in the current version have font sizes that are far too small for comfortable reading.

Response. We agree and regenerated all the figures.

Major Comment 8: Missing context for ITF variability (ENSO/IOD)

Was 2024 a neutral, El Niño, or La Niña year? The authors should compare their observations to the long-term mean or at least to the 2023–2024 ENSO/IOD phase.

Response. We added the ENSO and IOD context to Sect. 3.2, using the NOAA Oceanic Niño Index and the Australian Bureau of Meteorology IOD index. The record began during a strong El Niño and just after a strong positive IOD event, and conditions were neutral for most of 2024.

We do not have a multi-year in situ or reanalysis baseline at the mooring site, so we cannot quantify how representative this year was. We state this as a limitation instead of claiming representativeness.

> **Revised text in Sect. 3.2:**

"The record spans an interannual transition. A strong El Niño peaked in boreal winter 2023/24 (Oceanic Niño Index of 2.0 for November–January, remaining at or above 0.5 until March–May 2024; NOAA Climate Prediction Center), followed by ENSO-neutral conditions for the rest of 2024 (index of −0.3 to −0.4 at the end of the record). A strong positive Indian Ocean Dipole event peaked in October 2023 (weekly index +1.92°C) and decayed by early 2024, after which the dipole remained neutral apart from a short negative excursion from mid-October to November 2024 (Australian Bureau of Meteorology). The first months of the record therefore followed a combined El Niño and positive-dipole state, and the thermocline deepening through 2024 coincided with the return to neutral conditions. No multi-year baseline is available at the site, so the representativeness of this year cannot be quantified here."